Regenerative Therapy 26 (2024) 180–187

Contents lists available at ScienceDirect

Regenerative Therapy

journal homepage: http://www.elsevier.com/locate/reth

Original Article

# Skeletal muscle injury treatment using the Silk Elastin® injection in a rat model

Kyohei Nakata [a, *], Masakazu Ishikawa [b], Naosuke Kamei [a], Shigeru Miyaki [c], Nobuo Adachi [a], Keiichiro Inoue [d], Shingo Kawabata [d]

[a] Department of Orthopaedic Surgery, Graduate School of Biomedical and Health Sciences, Hiroshima University Hospital, Japan
[b] Department of Orthopaedic Surgery, Faculty of Medicine, Kagawa University Hospital, Japan
[c] Medical Center for Translational and Clinical Research, Hiroshima University Hospital, Japan
[d] Sanyo Chemical Industries, LTD., Japan

ARTICLE INFO

*Article history:*
Received 1 January 2024
Received in revised form
4 May 2024
Accepted 19 May 2024

*Keywords:*
Skeletal muscle
Injury
Material
Fibrosis

ABSTRACT

*Background:* Skeletal muscle injury (SMI) is often treated conservatively, although it can lead to scar tissue formation, which impedes muscle function and increases muscle re-injury risk. However, effective interventions for SMIs are yet to be established.
*Hypothesis:* The administration of Silk Elastin® (SE), a novel artificial protein, to the SMI site can suppress scar formation and promote tissue repair.
*Study design:* A controlled laboratory study.
*Methods:* *In vitro*: Fibroblast migration ability was assessed using a scratch assay. SE solution was added to the culture medium, and the fibroblast migration ability was compared across different concentrations. *In vivo*: An SMI model was established with Sprague–Dawley rats, which were assigned to three groups based on the material injected to the SMI site: SE gel (SE group; n = 8), atelocollagen gel (Atelo group; n = 8), and phosphate buffer saline (PBS group; n = 8). Histological evaluations were performed at weeks 1 and 4 following the SMI induction. In the 1-week model, we detected the expression of transforming growth factor (TGF)-β1 in the stroma using immunohistological evaluation and real-time polymerase chain reaction analysis. In the 4-week model, we measured tibialis anterior muscle strength upon peroneal nerve stimulation as a functional assessment.
*Results:* *In vitro*: The fibroblast migration ability was suppressed by SE added at a concentration of $10^4$ μg/mL in the culture medium. *In vivo*: In the 1-week model, the SE group exhibited significantly lower TGFβ −1 expression than the PBS group. In the 4-week model, the SE group had a significantly larger regenerated muscle fiber diameter and smaller scar formation area ratio than the other two groups. Moreover, the SE group was superior to the other two groups in terms of regenerative muscle strength.
*Conclusion:* Injection of SE gel to the SMI site may inhibit tissue scarring by reducing excessive fibroblast migration, thereby enhancing tissue repair.
*Clinical relevance:* The findings of this study may contribute to the development of an early intervention method for SMIs.


## 1. Introduction

Skeletal muscle injuries (SMIs) are the most common sport-related injuries. The frequency of SMIs is approximately 30%, and complete recovery typically occurs over a prolonged period [1,2,3,4]. Soccer players require more than 60 days to recover from muscle injuries before returning to the game; furthermore, long-term activity restrictions may be necessary. However, high recurrence rates after returning to competition have been reported [5], and functional decline remains a clinical challenge not only in the field of sports but also after surgery performed to address these injuries [6,7].

Acute muscle injury is typically treated conservatively with rest, ice, compression, and elevation (RICE); no interventional treatments

* Corresponding author. Department of Orthopaedic Surgery, Graduate School of Biomedical and Health Sciences, Hiroshima University, 1-2-3 Kasumi, Minami-ku, Hiroshima, 734-8551, Japan.
Peer review under responsibility of the Japanese Society for Regenerative Medicine.

https://doi.org/10.1016/j.reth.2024.05.012

have been established. Although hematoma aspiration, steroid injections, plate-rich plasma (PRP) injections, and extracorporeal shockwave therapy (ESWT) have been shown to achieve good clinical results in a few cases, promising therapeutic options remain elusive [8,9,10,11].

Silk Elastin® (SE) is an artificial protein produced using recombinant DNA technology that combines repeats of a silk-fibroin-derived sequence (GAGAGS), which contributes to hydrophobicity, material processing, and strength, and an elastin-derived sequence (GVGVP), which is primarily associated with elasticity [4]. By adjusting the composition of these elements, SE enables the fabrication of various material forms such as gels, sheets, sponges, and microfibers. SE exhibits excellent biocompatibility. Previous studies have shown its potential to promote wound healing, and a clinical trial examining SE as a wound dressing material has demonstrated its safety and efficacy [7,12,11]. These studies have concluded that SE gel could be used as a scaffold to enhance soft tissue repair and prevent scar tissue formation.

Here, we hypothesize that administering SE gel to the SMI site can prevent scar tissue formation and accelerate the healing process. The objective of the present study was to investigate the effect of SE gel administration on skeletal muscle regeneration in a rat SMI model.

## 2. Material and methods

### 2.1. Experimental animals

The Ethics Committees for Experimental Animals approved all animal procedures, and all animals were treated according to the guidelines of the Institutional Animal Care and Use Committee (A17-102). Experiments were performed using 12-week-old male Sprague–Dawley rats (CLEA Japan Inc., Meguro-Ku, Tokyo, Japan; http://www.clea-japan. com). They were fed a standard diet and provided continuous access to water.

### 2.2. Silk elastin

SE is an artificial protein comprising silk fibroin sequences, contributing to hydrophobicity, material processing, and strength, and elastin sequences primarily involved in elasticity. By adjusting the composition of these elements, SE can be fabricated into various material forms, including gels, sheets, sponges, and microfibers. SE is recognized as a material with high cell affinity. SE used in the current study was provided by Sanyo Chemical Industries, Ltd. Hydrophilic SE was dissolved in phosphate-buffered saline (PBS), assuming the specific gravity of PBS to be 1.0 g/mL, and the concentration was calc1ulated using weight ratios.

### 2.3. In vitro: fibroblast migration assay

The tibialis anterior muscles (TA) of 12-week-old Sprague–Dawley rats were harvested and minced, and fibroblasts were isolated and cultured as described previously [13]. The muscles were seeded in a 10-cm culture dish with 1% fetal bovine serum (FBS), L-glutamine, and mitomycin C. Three days after seeding, the fibroblasts migrated from the muscle; these cells were used in passage 2. The fibroblasts were seeded in a 6-well plate, with $3.0 \times 10^5$ fibroblasts in each well. When the fibroblast density in each well reached 90%, FBS with mitomycin C was added to stop the culture growth.

Fibroblast migration was analyzed using the scratch assay. After scratching the bottom of the well using a 1000-μL pipette chip, 1% FBS containing SE was added as the cultured medium. SE at various concentrations (0, $10^{-1}$, $10^1$, $10^3$, and $10^4$ μg/mL) was added thereafter. A rectangular, acellular area scratched at time 0 was set as 100%. After 24 and 48 h, the area of migrating cells was measured using the ImageJ software (National Institutes of Health, Bethesda, MD, http://www.nih.gov), and the ratio of the migrating cell area to the time 0 area was calculated [Figs. 1 and 2].

### 2.4. In vivo: SMI model of rats

All rats were anesthetized with ketamine and xylazine (60 and 10 mg/kg, respectively), and adequate level of anesthesia was maintained during the surgical procedure. As described previously, an anterolateral skin incision was made in the left leg, and the TA was exposed. The fascia was incised longitudinally and carefully released from the muscle belly. The muscle belly of the TA was lacerated transversely at the mid portion using a surgical knife. The defect shape was constantly a wedge, 5 mm in depth, 4 mm in width, and 6 mm in length. After closing the fascia with sutures, a single local injection of 50 μL of SE gel was administered to the muscle defect. PBS and atelocollagen gel (Atelo) were administered in the same manner to rats in the two other groups ($n = 8$ rats/group). The skin was sutured, and the rats were placed in their cages with no restriction on mobility. The second operation was performed 1 and 4 weeks after the first operation. These operations were performed by making an anterolateral skin incision with the rats under general anesthesia, as performed in the initial surgery. Subsequently, the rats were euthanized by administering an anesthesia overdose, and the TA was harvested. Prior to sacrifice, muscle strength was assessed 4 weeks after the initial surgery.

### 2.5. Processing of the regenerated muscle tissue

After harvesting the TA, longitudinal-axis sections were cut using a surgical knife, with the injured portion at the center. The rest of the muscle sample was cut in half along the short axis at the muscle injury to prepare cross-sections. The obtained sections were immediately embedded in a tissue-freezing medium (Triangle Biomedical Sciences, Durham, NC; http://www.trianglebiomedical.com) and frozen using liquid nitrogen. After medium hardening, the sections were stored at −80 °C for subsequent histological and immunofluorescent staining.

### 2.6. Histological evaluation

The frozen muscle sample was cut into 8-μm sections. Hematoxylin–eosin (HE) staining was performed to calculate the diameter and density per unit area of the regenerated muscle in the cross-section of the injury. Regenerated myofiber was defined as a tissue form with centronuclear myofiber. For evaluating muscle regeneration, the total number and diameter of centronuclear myofibers were measured within the injured site of each sample using a previously described protocol [14,15]. Measurements were performed at five randomly designated observation points from the edge, bottom, and middle sections of the wound site, and the average value was calculated.

Tissue samples were harvested 1 and 4 weeks post-injury in the PBS, Atelo, and SE groups. Photographs were obtained using a microscope and imported into a computer using Adobe Photoshop (Adobe Systems Inc., San Jose, CA,; http://www.adobe.com). The scar area ratio was measured using Masson-Trichrome-stained longitudinal sections. The ratio of scar tissue volume to muscle tissue volume was calculated. The three primary colors were separated using the software; the blue area was measured as scar tissue and the red area was measured as muscle tissue.

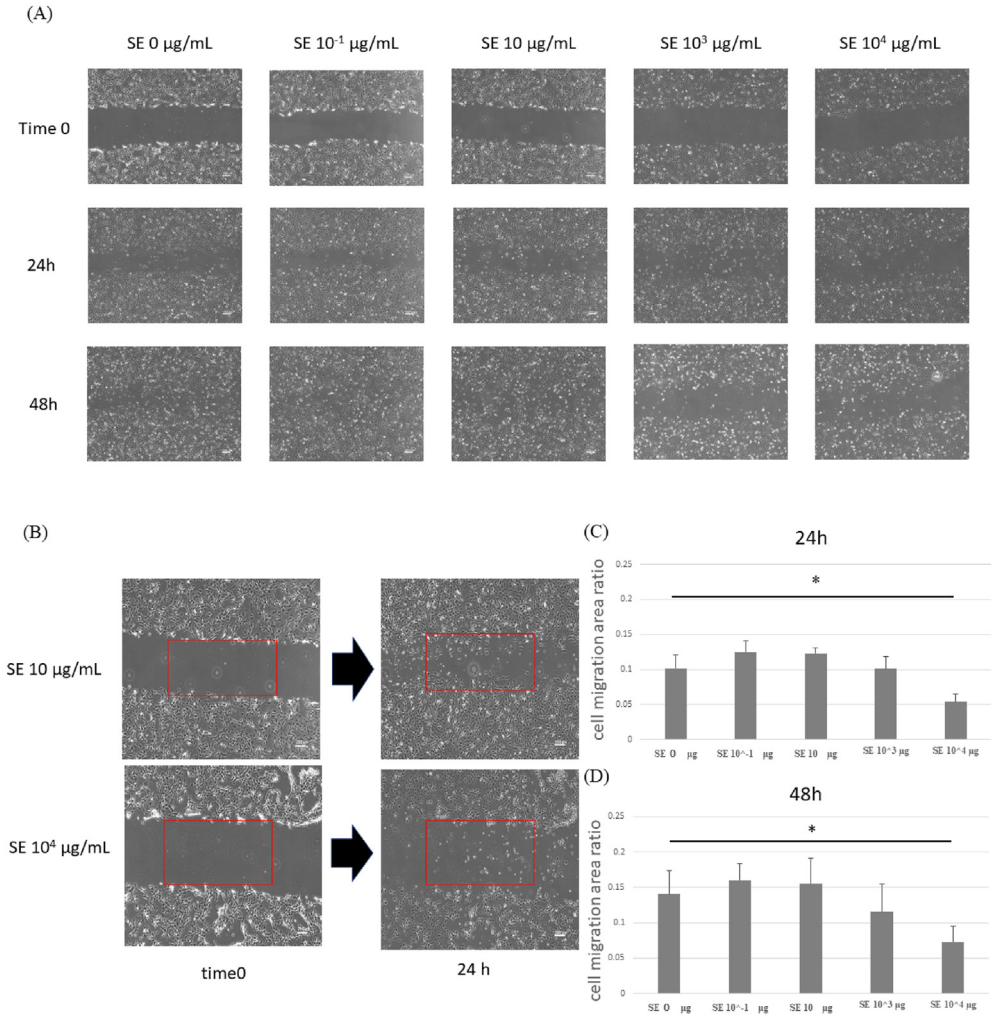


**Fig. 1.** (A) Migration assay of skeletal muscle fibroblasts. Fibroblasts were seeded in 6-well plates, and silk-elastin (SE) gel was added to the medium at concentrations of 0, $10^1$, $10^1$, $10^3$, and $10^4$ μg/mL. (B) At 24 and 48 h after scratching the bottom of the wells, the area was photographed under a microscope to assess the cells that had migrated to the acellular field. (C), (D) Graph of migration assay results. At both 24 and 48 h, the ratio of the cell migration area was reduced in the medium with $10^4$ μg/mL SE compared with that of fibroblast migration area in the medium without SE.

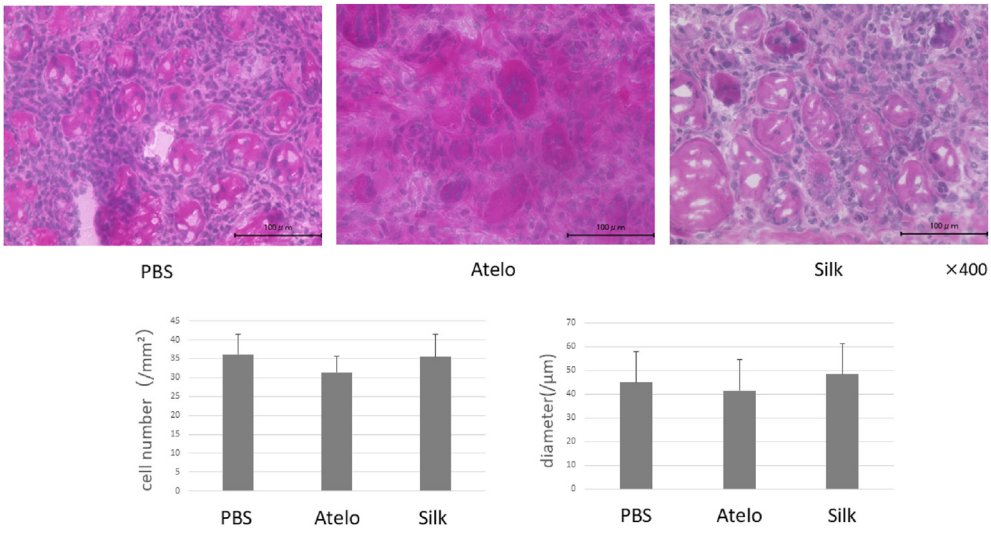


**Fig. 2.** Axial sections of injured skeletal muscle stained with hematoxylin–eosin 1 week post-injury. The number of regenerating muscles with a central core and the diameter of the regenerating muscle fibers per $mm^2$ were measured, with no significant differences detected among the three groups. Atelo, atelocollagen gel; PBS, phosphate-buffered saline; SE, silk-elastin gel.

**Table 1**
Primers utilized in real time PCR.

| Gene | Rat-specific primer pair sequence for real-time PCR | Fragment length (bp) |
|---|---|---|
| *r TGF-β1* | F: 5′-CCACGTGGAAATCAATGGGA-3′<br>R: 5′-GGCCATGAGGAGCAGGAAG-3′ | 91 |
| *r Pax7* | F: 5′-GCCCTCAGTGAGTTCGATTAGC-3′<br>R: 5′-TCCTTCCTCATCGTCCTCTTTC-3′ | 70 |
| *r MyoD* | F: 5′-GCGACAGCCGATGACTTCTAT-3′<br>R: 5′-GGTCCAGGTCCTCAAAAAAGC-3′ | 73 |

### 2.7. Immunostaining evaluation

The injured area was subjected to immunohistochemical staining with transforming growth factor (TGF)-β1, a main signal for fibrosis. The tissue cross sections were cut into 8-μm sections and fixed in 4% para formalin solution. The slides were blocked with 10% goat serum. Following overnight treatment with the TGF-β1 primary antibody (ab215715; Abcam), the tissue sections were incubated with a secondary antibody (goat-anti rabbit 594, ab15537; Abcam) for 2 h. Finally, the nucleus was stained with DAPI. Photographs were obtained using a polarizing microscope and imported into a computer. The three primary colors were separated, and the amount of red light emitted in the tissue stroma of the cross-section was quantified.

### 2.8. Electromechanical evaluation

To evaluate muscle function, we measured the isometric tensile strength produced by stimulating the peroneal nerve as described previously [15]. Muscular strength comprises two elements: maximum contraction force and muscular endurance. The tetanus ratio indicates the ratio of maximum contraction force on the affected side to that on the healthy side. The twitch ratio compares muscle contraction force during frequent stimulation to that on the healthy side.

Before harvesting the TA muscle of the 4-week SMI model rats, all rats were placed in the supine position under general anesthesia. Following the placement of an anterolateral longitudinal skin incision on both legs, the TA muscles and peroneal nerves were exposed. The legs were fixed using a leg holder, and the peroneal nerves were stimulated with a stimulator (SEN2201; Nihon Koden, Tokyo, Japan, http//www.nihonkohden.co.jp). The stimulation frequency was 1 Hz (fast-twitch) and 50 Hz (tetanus). To determine the voltage of stimulation, the minimum voltage that visibly contracted the TA was measured as a threshold. The nerve was then stimulated with a voltage that was 10-fold higher than that of the threshold, and the maximum isometric tensile strength produced by the TA of both legs was measured, and the ratio of strength was calculated.

### 2.9. Real-time polymerase chain reaction analysis

Intrinsic factors in the regenerated muscles of rats were detected by performing real-time polymerase chain reaction (PCR). On day 7, specimens were harvested and analyzed. Real-time PCR detection was performed using the ΔCT method, with the median of the PBS group set as 1 for comparative analysis. Real-time PCR was performed using a Mini Opticon System (Bio-Rad) with QuantiTect SYBR Green (Qiagen KK, Tokyo, Japan; http://www.qiagen.co.jp) according to the manufacturer's protocol, using rat-specific primers (Table 1).

### 2.10. Statistical analyses

All data are expressed as mean ± standard deviation (SD). The three groups were compared using a one-way analysis of variance, followed by the post-hoc Tukey–Kramer's test. Results with P-values of <0.05 were considered statistically significant.

## 3. Results

In the *in vitro* migration assay, fibroblast migration was suppressed by SE gel at a concentration of $10^4$ μg/mL [Fig. 1].

Considering the histological evaluation of tissue sections obtained at 1 week post-SMI induction, there were no significant differences in the diameter of centronuclear myofibers or the number of cells (diameter, PBS group vs. Atelo group vs. SE group: 36.1 ± 5.3 μm vs. 31.4 ± 4.2 μm vs. 35.4 ± 5.9 μm; number of cells, PBS group vs. Atelo group vs. SE group: 45.0 ± 13.2/$mm^2$ vs. 41.5 ± 12.3/$mm^2$ vs. 48.3 ± 13.0/$mm^2$) [Fig. 2].

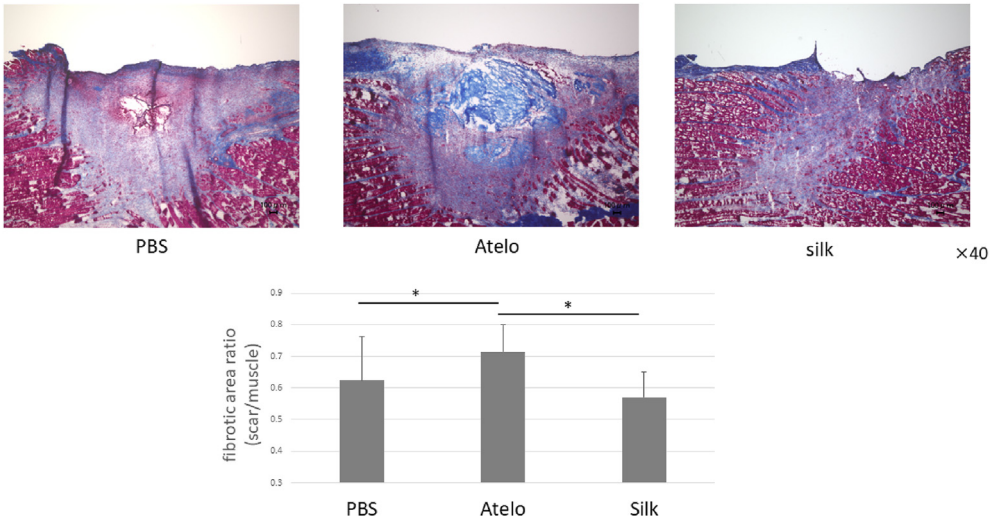


**Fig. 3.** Sagittal sections of injured skeletal muscle stained with Masson trichrome 1 week post-injury. The area of muscle fibers and scar tissue was measured using ImageJ, and the area ratio of scar tissue to muscle fibers was calculated. The ratio of scar tissue area in the atelocollagen group was significantly greater than that in the other two groups. Atelo, atelocollagen gel; PBS, phosphate-buffered saline; SE, silk-elastin gel.

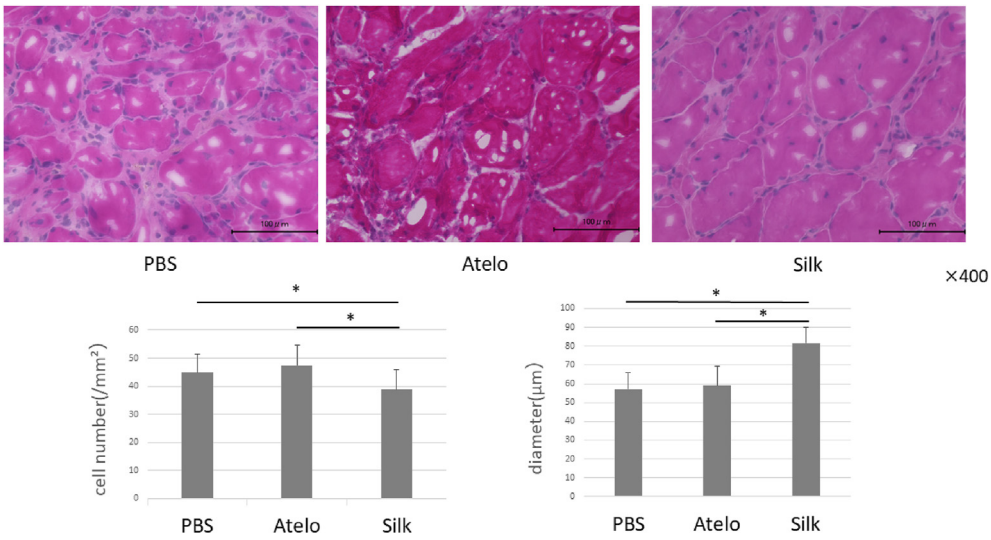


**Fig. 4.** Axial sections of injured skeletal muscle stained with hematoxylin–eosin 4 weeks post-injury. The silk-elastin group had significantly fewer regenerating muscles than the other two groups, whereas the diameter of regenerating muscles was significantly greater than that in the other groups. Atelo, atelocollagen gel; PBS, phosphate-buffered saline; SE, silk-elastin gel.

The Masson trichrome staining results revealed that the ratio of scar tissue to muscle tissue was significantly higher in the Atelo group than in the other two groups (PBS group: 0.62 ± 0.13; Atelo group: 0.71 ± 0.08; SE group: 0.56 ± 0.09) [Fig. 3].

In the four-week post-injury evaluation, the SE group exhibited a significantly larger myofiber diameter than the other two groups (PBS group: 57.0 ± 8.7 μm; Atelo group: 59.1 ± 10.32 μm; SE group: 81.7 ± 8.3 μm), although the number of regenerated myofibers was significantly lower (PBS group: 44.9 ± 6.4/mm$^2$; Atelo group: 47.3 ± 7.3/mm$^2$; SE group: 38.8 ± 7.2/mm$^2$) [Fig. 4].

Examination of longitudinal sections, revealed that the SE group had a significantly lower ratio of scar tissue area than the other two groups, with the atelocollagen group exhibiting the highest ratio (PBS group: 0.63 ± 0.06, Atelo group: 0.69 ± 0.15, SE group: 0.47 ± 0.08). In the Atelo group, Atelo was retained at the site of muscle injury, whereas in the SE group, no SE was retained at the injury site [Fig. 5].

In the 4-week post-injury evaluation, we measured the muscle strength of the affected side relative to that of the unaffected side. The SE group exhibited significantly superior fast-twitch and tetanus ratios compared to the other groups (twitch ratio, PBS group vs. Atelo group vs. Se group: 0.67 ± 0.15 vs. 0.59 ± 0.07 vs. 0.75 ± 0.12; tetanus ratio, PBS group vs. Atelo group vs. Se group: 0.64 ± 0.14 vs. 0.57 ± 0.07 vs. 0.77 ± 0.11) [Fig. 6].

In the 1-week post-injury evaluation using fluorescent immunostaining, we measured stromal TGF-β1 expression in the coronal tissues. The SE group exhibited significantly lower TGF-β1 expression than the other groups (PBS group: 9.6 ± 3.4; Atelo group: 8.3 ± 3.7; SE group: 6.1 ± 3.3). Based on real-time PCR analysis, TGF-β1 expression was significantly reduced in both Atelo (0.55 ± 0.39) and SE (0.48 ± 0.30) groups compared with that in the PBS group (1.06 ± 0.46) [Fig. 7].

The mRNA expression of PAX7 and MyoD in the scar tissue 7 days after muscle injury was measured using real-time PCR. There

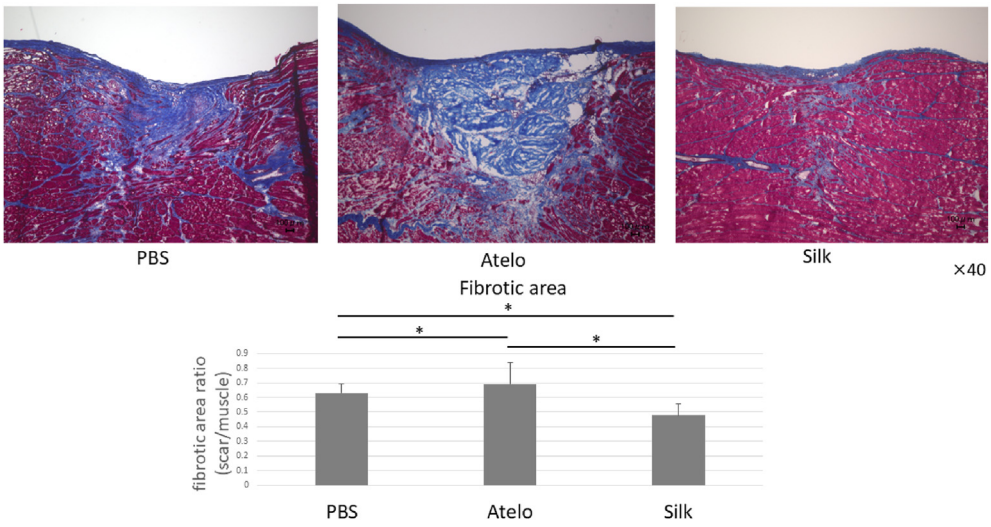


**Fig. 5.** Sagittal sections of injured skeletal muscle stained with Masson trichrome 4 weeks post-injury. The ratio of scar tissue area in the Atelo group was significantly greater than that in the other two groups. The ratio of scar tissue area in the SE group was significantly smaller than that in the other two groups. Atelo, atelocollagen gel; PBS, phosphate-buffered saline; SE, silk-elastin gel.

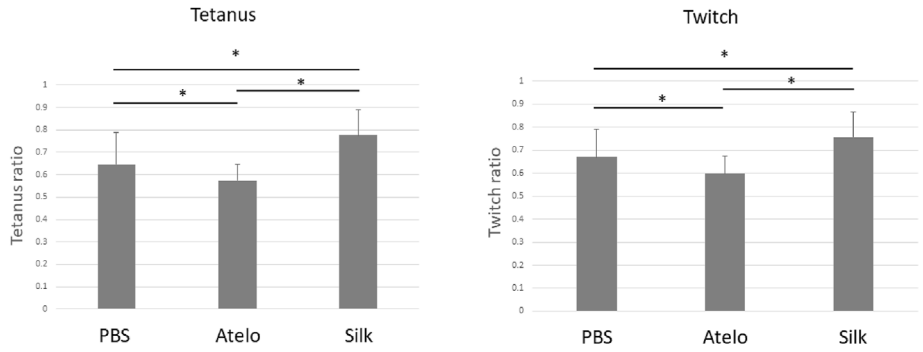


**Fig. 6.** Isometric tensile strength of the tibialis anterior muscle during electronic peroneal nerve stimulation at 1 Hz (twitch) and 50 Hz (tetanus). The strength of the injured muscle was assessed as a ratio to the strength of the muscle on the uninjured side. In both types of electrical stimulation, the Atelo group had a significantly weaker muscle strength than the other two groups, and the SE group showed significantly stronger muscle strength than the other two groups. Atelo, atelocollagen gel; PBS, phosphate-buffered saline; SE, silk-elastin gel.

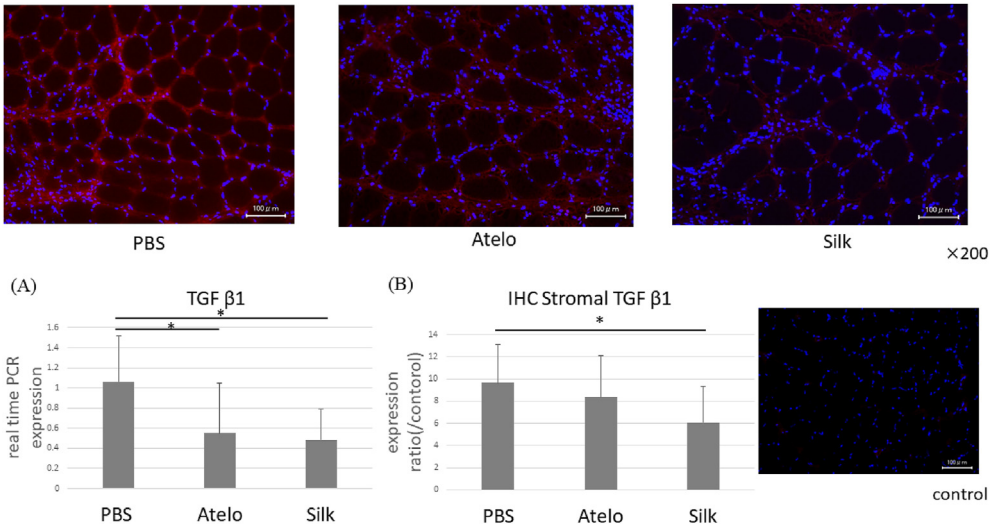


**Fig. 7.** (A) Real-time PCR analysis revealed reduced TGF-β1 expression in the SE group. Atelo, atelocollagen gel; PBS, phosphate-buffered saline; SE, silk-elastin gel. (B) Immunostaining for TGF-β1 in coronal section tissues 1 week post-muscle injury. The TGF-β1 positive area was significantly smaller in the SE group than in the PBS group.

were no significant differences in the expression level of either PAX7 or MyoD among the three groups [Fig. 8].

## 4. Discussion

Our findings suggest that early administration of SE to the SMI site may promote tissue repair by inhibiting excessive fibroblast accumulation and scar formation. It is well-known that substantial scarring of regenerated muscle tissues occurs in the presence of fissure damage beyond the repair capacity [16]. Regarding studies that have focused on preventing scar formation, Terada et al. reported that losartan can enhance the success of myoblast transplantation by secondarily antagonizing TGF-β1 and inhibiting muscle fibrosis [17]. In addition, Hara et al. have demonstrated that post-neutralizing antibodies that inhibit fibroblast adhesion can decrease the occurrence of fibrosis post-SMI [13]. They found that muscle fibrosis suppresses myofiber regeneration.

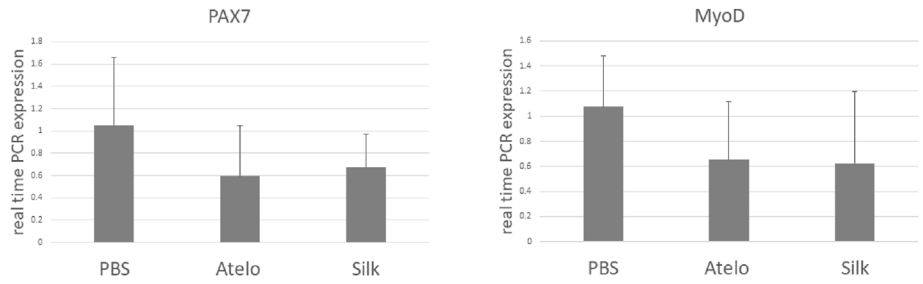


**Fig. 8.** mRNA expression levels of PAX7 and MyoD in the scar tissue at 1 week after muscle injury were measured using real-time PCR and the ΔCT method with the median value of PBS as 1.

Herein, we described the characteristics of SE. SE can be processed into various forms and has been used in clinical practice with a high safety profile. SE has been used to treat intractable ulcers and clinical trials have been conducted [18]. SE is characterized by its ability to be processed into various forms, such as gel, sponge, and sheet. Here, gel-type SE was administered to treat injured muscles. Considering its effects on fibroblasts, Somamoto et al. reported that SE inhibits the adhesion of fibroblasts without apoptosis *in vitro* [19].

The mechanism of fibrosis inhibition needs to be considered. Christopher et al. noted that during the healing process post-SMI, an excessive inflammatory response or prolonged inflammatory response causes insufficient tissue repair and scar formation [16]. TGF-β1 is recognized as an important signal in the fibrotic cascade in muscle injury [20,21]. The abundant presence of TGF-β1 in platelets is well-established; hence, TGF-β1 is primarily released from platelets at the muscle injury site [22]. Here, the expression of TGF-β1 was significantly reduced in the SE group compared with that in the PBS group, as evidenced in the immunohistological evaluation.

In real-time PCR analysis, both Atelo and SE groups exhibited a significant decrease in TGFβ-1 expression compared to the PBS group [Fig. 7]. This disparity in results between the assessment methods, i.e., immunohistochemistry and real-time PCR, could be attributed to the difference in evaluation sites. Specifically, immunostaining was used to evaluate the regenerated tissue surrounding the scar, whereas specimens collected for real-time PCR included a small quantity of the scar tissue itself, potentially leading to differences in results. Nevertheless, the SE group exhibited a significant decrease in TGF-β expression when compared with the PBS group, regardless of the methodology. We also evaluated the mRNA expression levels of PAX7 and MyoD as markers of muscle tissue repair[11,34]. However, there were no significant differences between the SE group and the other two groups. Inhibition of scar formation, rather than promotion of muscle tissue repair, may be the dominant mechanism for repair of injured skeletal muscle upon administration of SE.

Based on the *in vitro* results, SE may inhibit fibroblast migration to the injured site. We hypothesize that the SE gel suppresses the infiltration of excessive fibroblasts and inflammatory cells during the early phase, from 2 to 3 days post-surgery, thereby suppressing the scarring of the repair tissue.

Regarding the myogenic effect, the concentration gradually decreased after *in vivo* administration, and the problematic inhibition of the myogenic effect did not occur. SE has been shown to promote the migration of mouse-derived fibroblasts and collagen production at low concentrations, suggesting that SE may exhibit distinct functional properties depending on its concentration [23]. In the present study, the persistence duration of SE may have differed from that of Atelo. At the 4-week tissue evaluation, we found that Atelo was retained in the tissue, suggesting that it may inhibit muscle fiber repair. Notably, SE disappeared earlier than Atelo, with no SE was detected in tissues collected at 4 weeks. The earlier disappearance of SE, compared with that of Atelo, may have favored the repair of the injured areas of the muscle without interfering with muscle repair.

The timing of administration also warrants discussion. Previous studies have selected distinct administration timings according to the mechanism of inhibition of scar formation [24,13,17]. In the present study, the SE gel injection was performed at the time of SMI modeling. In our study, the SE gel physically suppressed the migration of fibroblasts and the accumulation of platelets and neutrophils from which cytokines are derived, whereas other reports have indicated the pharmacological suppression of fibroblast activity. Considering the timing of the inflammation phase when hematoma formation occurs and the early absorption characteristics of SE gels, we believe that the administration of SE gel at the time of SMI modeling was effective.

In this study, we chose atelocollagen as the experimental control. SE is a pure material and does not contain cells or humoral factors such as growth factors; therefore, atelocollagen, the most commonly used material in tissue engineering, was considered suitable as an experimental control. As platelet-rich plasma (PRP) has been widely used in clinical practice and its efficacy in skeletal muscle repair has been reported, the difference in efficacy between SE and PRP should also be discussed [22,9]. However, the properties of PRP vary depending on the leukocyte content and donor, and some studies have raised concerns about the efficacy of PRP in repairing skeletal muscle injury [22,8,3,25]. The optimal conditions under which PRP can promote skeletal muscle repair have not yet been determined, and it is difficult to compare differences in efficacy between SE and PRP.

Finally, considering the benefits of administering SE in gel form, Kiran et al. demonstrated the advantages of hydrogel properties. Hydrogels can be delivered using less invasive approaches [26]. In recent years, accurate injection into the injured site has been achieved using the echo-guided intervention technique. Percutaneous interventions such as blood aspiration and PRP injections for skeletal muscle injuries with large hematomas have been reported, and the inhibition of hematoma formation is crucial for promoting good tissue repair [12]. The injectable SE gel can be administered to the injured area rapidly and in limited quantity [27]. Moreover, the results of the present study may lead to a novel therapy capable of suppressing hematoma formation and promoting tissue repair by combining hematoma aspiration therapy with SE administration.

## 5. Conclusions

SE administration to the SMI model rats suppressed scar tissue formation and promoted muscle repair at 4 weeks post-injury. SE-mediated inhibition of TGF-β1 expression and fibroblast migration at the muscle injury site may involve the promotion of muscle repair.

## 6. Limitations

First, this study was performed using a small number of rats. Second, changes beyond 4 weeks post-injury were not examined. Finally, the Atelo group retained Atelo gel even at 4 weeks post-injury, and this aspect may have been excluded in the accurate scar area evaluation method used in this study. However, considering the perspective that remaining Atelo gel may inhibit tissue repair, we opted to measure it similar to scar tissue for assessment.

## Declaration of competing interest

The authors declare the following financial interests/personal relationships which may be considered as potential competing interests: Kyohei Nakata reports equipment, drugs, or supplies was provided by Hiroshima University Hospital. Silk elastin is provided by Sanyo Chemical Industries, Ltd. If there are other authors, they declare that they have no known competing financial interests or personal relationships that could have appeared to influence the work reported in this paper.

## References

[1] Askling CM, Tengvar M, Tarassova O, Thorstensson A. Acute hamstring injuries in Swedish elite sprinters and jumpers: a prospective randomised controlled clinical trial comparing two rehabilitation protocols. Br J Sports Med 2014;48(7):532–9.
[2] Ekstrand J, Hagglund M, Walden M. Epidemiology of muscle injuries in professional football (soccer). Am J Sports Med 2011;39(6):1226–32.
[3] Gabbe BJ, Bennell KL, Finch CF, Wajswelner H, Orchard JW. Predictors of hamstring injury at the elite level of Australian football. Scand J Med Sci Sports 2006;16(1):7–13.

[4] Ishoi L, Krommes K, Husted RS, Juhl CB, Thorborg K. Diagnosis, prevention and treatment of common lower extremity muscle injuries in sport - grading the evidence: a statement paper commissioned by the Danish Society of Sports Physical Therapy (DSSF). Br J Sports Med 2020;54(9):528–37.
[5] Orchard J, Seward H. Epidemiology of injuries in the Australian football league, seasons 1997-2000. Br J Sports Med 2002;36(1):39–44.
[6] Grogan BFHJ. Skeletal trauma research consortium. Volumetric muscle loss. J Am Acad Orthop Surg 2011;19(Suppl 1):S35–7.
[7] Morgan JPM, Hamm M, Schmitz C, Brem MH. Return to play after treating acute muscle injuries in elite football players with radial extracorporeal shock wave therapy. J Orthop Surg Res 2021;16(1):708.
[8] Dimauro I, Grasso L, Fittipaldi S, et al. Platelet-rich plasma and skeletal muscle healing: a molecular analysis of the early phases of the regeneration process in an experimental animal model. PLoS One 2014;9(7):e102993.
[9] Hotfiel T, Seil R, Bily W, et al. Nonoperative treatment of muscle injuries - recommendations from the GOTS expert meeting. J Exp Orthop 2018;5(1):24.
[10] McCarthy E, Hegazi TM, Zoga AC, et al. Ultrasound-guided interventions for core and hip injuries in athletes. Radiol Clin 2016;54(5):875–92.
[11] Zissler A, Steinbacher P, Zimmermann R, et al. Extracorporeal shock wave therapy accelerates regeneration after acute skeletal muscle injury. Am J Sports Med 2017;45(3):676–84.
[12] Trunz LM, Landy JE, Dodson CC, et al. Effectiveness of hematoma aspiration and platelet-rich plasma muscle injections for the treatment of hamstring strains in athletes. Med Sci Sports Exerc 2022;54(1):12–7.
[13] Hara M, Yokota K, Saito T, et al. Periostin promotes fibroblast migration and inhibits muscle repair after skeletal muscle injury. J Bone Joint Surg Am 2018;100(16):e108.
[14] Natsu KOM, Mochizuki Y, Hachisuka H, Yanada S, Yasunaga Y. Allogeneic bone marrow-derived mesenchymal stromal cells promote the regeneration of injured skeletal muscle without differentiation into myofibers. Tissue Eng 2004;10(7–8):1093–112.
[15] Shi M, Ishikawa M, Kamei N, et al. Acceleration of skeletal muscle regeneration in a rat skeletal muscle injury model by local injection of human peripheral blood-derived CD133-positive cells. Stem Cell 2009;27(4):949–60.
[16] Mann CJ, Perdiguero E, Kharraz Y, et al. Aberrant repair and fibrosis development in skeletal muscle. Skeletal Muscle 2011;1(1):21.
[17] Terada S, Ota S, Kobayashi M, et al. Use of an antifibrotic agent improves the effect of platelet-rich plasma on muscle healing after injury. J Bone Joint Surg Am 2013;95(11):980–8.
[18] Noda K, Kawai K, Matsuura Y, et al. Safety of silk-elastin sponges in patients with chronic skin ulcers: a phase I/II, single-center, open-label, single-arm clinical trial. Plast Reconstr Surg Glob Open 2021;9(4):e3556.
[19] Somamoto S. An artificial Silk-elastin-like protein suppresses cells adhesion without apoptosis. J Biotechnol Biomater 2012;2:139.
[20] Darakhshan S, Pour AB. Tranilast: a review of its therapeutic applications. Pharmacol Res 2015;91:15–28.
[21] Mahdy MAA, Warita K, Hosaka YZ. Neutralization of transforming growth factor (TGF)-beta1 activity reduced fibrosis and enhanced regeneration of glycerol-injured rat muscle. J Vet Med Sci 2020;82(2):168–71.
[22] Carnes ME, Pins GD. Skeletal muscle tissue engineering: biomaterials-based strategies for the treatment of volumetric muscle loss. Bioengineering (Basel) 2020;7(3):85.
[23] Hu X, Park SH, Gil ES, et al. The influence of elasticity and surface roughness on myogenic and osteogenic-differentiation of cells on silk-elastin biomaterials. Biomaterials 2011;32(34):8979–89.
[24] Chan YS, Li Y, Foster W, Fu FH, Huard J. The use of suramin, an antifibrotic agent, to improve muscle recovery after strain injury. Am J Sports Med 2005;33(1):43–51.
[25] Kawabata S, Kanda N, Hirasawa Y, et al. The utility of silk-elastin hydrogel as a new material for wound healing. Plast Reconstr Surg Glob Open 2018;6(5):e1778.
[26] Kiran S, Dwivedi P, Kumar V, Price RL, Singh UP. Immunomodulation and biomaterials: key players to repair volumetric muscle loss. Cells 2021;10(8).
[27] Wang Y, Kankala RK, Cai YY, et al. Minimally invasive co-injection of modular micro-muscular and micro-vascular tissues improves in situ skeletal muscle regeneration. Biomaterials 2021;277:121072.